Comparison between numerical modeling and experimental measurements of the interface shape in Kyropoulos growth of Ti-doped sapphire crystals

Carmen Stelian, Gourav Sen, Nicolas Barthalay, Thierry Duffar

Comparison between numerical modeling and experimental measurements of the interface shape in Kyropoulos growth of Ti-doped sapphire crystals

C. Stelian [a,b,*], G. Sen [a], N. Barthalay [b], T. Duffar [a]

[a] SIMAP-EPM, 1340 Rue de la Piscine, BP 75, F-38402 Saint Martin d'Hères, France
[b] Le Rubis SA, BP 16, 38560 Jarrie, Grenoble, France

Numerical modeling is applied to investigate the factors affecting the shape of the crystal-melt interface during the growth of Ti-doped sapphire crystals by using the Kyropoulos method. Numerical results are compared to experimental visualization of the growth interface in the case of ingots grown in crucibles of 15 cm in diameter. The transient computations of the heat transfer and melt convection show that the interface curvature depends on the internal radiative effect in the sapphire crystal. The effective thermal conductivity increases significantly in the case of Ti-doped crystals, leading to conical shapes of the interface with large curvatures. The growth interface is less curved in the case of non-doped sapphire crystals which have a smaller absorption coefficient. The convection driven by buoyancy and Marangoni effects has also a strong effect on the interface shape. The intensity of the Marangoni flow increases significantly during the shouldering stage of the growth, leading to a more curved interface with a convex-concave shape. The comparison between numerically computed interface deflection and the experimental results shows a good agreement. According to present numerical analysis, the formation of a plateau and the temporal concave shape of the crystal are related to unfavorable thermal conditions at the beginning of the growth process.

1. Introduction

Large size sapphire crystals are usually grown by Kyropoulos, Czochralski, heat exchanger method (HEM) or controlled heat extraction system (CHES). The ingots grown by Kyropoulos method excel the competition in structural quality, size and production costs. The Kyropoulos furnace is designed to achieve low temperature gradients, owing to low dislocation density and good structural quality of crystals. Titanium doped sapphire crystals are of large interest as active media for the future high power laser chains [1,2].

Numerical modeling is a useful tool to investigate and optimize the Kyropoulos growth process. Several papers have been dedicated to the numerical analysis of the thermal field, stresses, melt convection and the shape of the crystal-melt interface [3–9]. In their work, Demina et al. [3,4] used numerical simulation to investigate the influence of the growth parameters on the temperature field, melt convection and the crystallization front shape. The formation of so-called "remelting zone" or "temporal concave shape of the crystal" during the shouldering stage of the growth is explained as an effect of two-vortex pattern of the flow. C.H. Chen et al. [5,6] investigated the influence of the input power in the heater on the melt convection and the shape of the crystal-melt interface. Other papers [7,8] have been dedicated to the analysis of the effect of the crucible geometry on the temperature field and convection in a Kyropoulos growth system. The effect of the Marangoni convection on the interface shape has been numerically investigated by Gao et al. [9]. They found that the Marangoni convection increases the curvature of the growth interface and influences the flow pattern, causing the temporal concave shape of the crystal. Although different models have been applied to simulate the internal radiation in the sapphire crystal [3–9], the influence of the internal radiative exchanges on the temperature and the flow field is not fully understood. The numerical studies in [5–9] apply steady-state computations to investigate the thermal and the flow field in the sample-crucible system at different stages of the growth process.

Ti-doped sapphire crystals of different dimensions have been

* Corresponding author at: SIMAP-EPM, 1340 Rue de la Piscine, BP 75, F-38402 Saint Martin d'Hères, France.
E-mail address: carmen.stelian@simap.grenoble-inp.fr (C. Stelian).

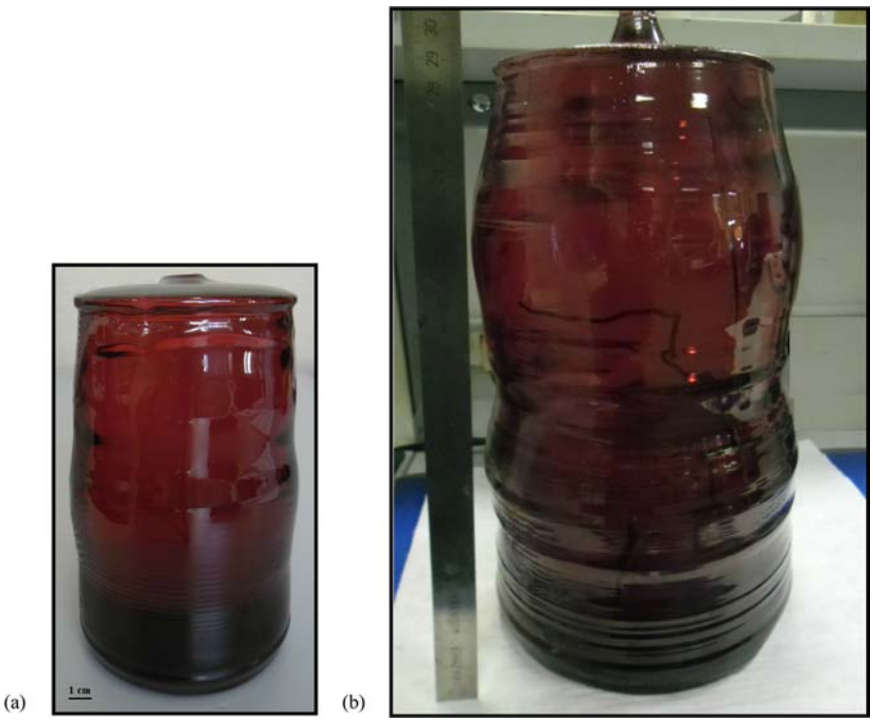

Fig. 1. Ti-doped sapphire crystals grown by Rubis SA Company in crucibles of various diameters: (a) d = 15 cm; (b) d = 30 cm.

Fig. 2. Shape of the crystals obtained by interrupting the growth process at time: (a) t = 31 h, τ = 4.5 cm/2.9 cm = 1.55; (b) t = 67 h, τ = 11 cm/4.3 cm = 2.55. Crucible diameter d = 15 cm.

successfully grown by Rubis SA Company (see Fig. 1). In the present work, transient numerical modeling is applied to investigate the coupled effects of the Marangoni flow and internal radiation on the shape of the crystal-melt interface. The numerical results are compared to experimental visualization of the growth interface performed in the case of Ti-doped crystals grown in crucibles of 15 cm in diameter.

2. Model description

The finite element software COMSOL Multiphysics is used for modeling the heat transfer and melt convection during the Kyropoulos growth of Ti-doped sapphire crystals. The simulation is performed in two steps. First, global modeling is applied to compute the evolution in time of the temperature field in the furnace, as well as the velocity field in the liquid sample. Then, the temperatures carried from the global computations are used as boundary conditions for an axisymmetric local model which includes the crystal, melt, crucible and the surrounding gas.

The governing equations of heat transfer and melt convection are:

$$\rho c_P \left(\frac{\partial T}{\partial t} + \vec{u} \cdot \nabla T \right) = k \nabla^2 T - Q_R \tag{1}$$

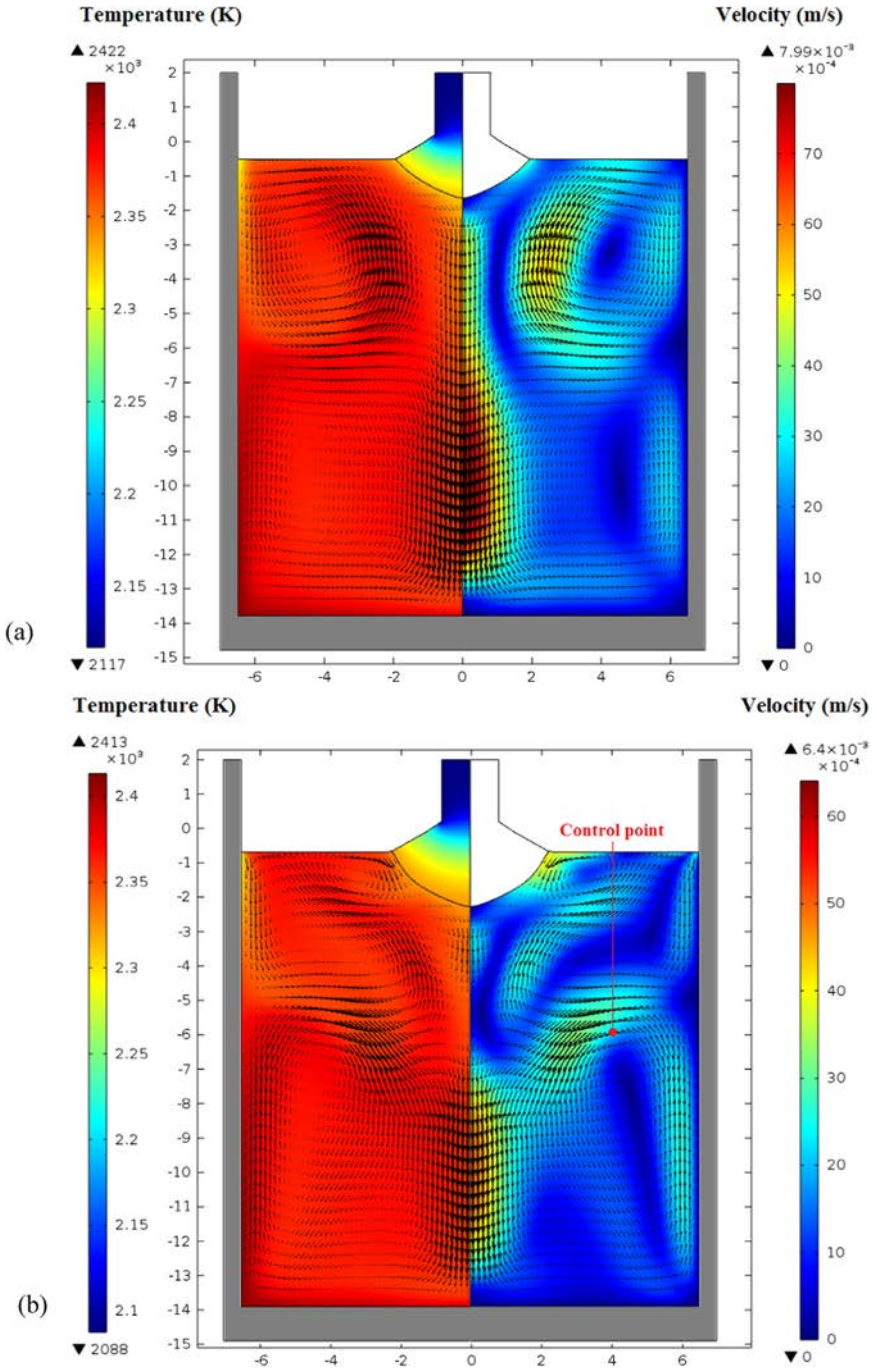

Fig. 3. Flow pattern in the melt at the beginning of the crystallization process: (a) without Marangoni convection ($\tau = 0.57$); (b) with Marangoni convection ($\tau = 0.73$). The color map shows the temperature field (left side) and the velocity field (right side). Computations without internal radiative effect.

$$\rho\left[\frac{\partial\vec{u}}{\partial t} + (\vec{u}\cdot\nabla)\vec{u}\right] = -\nabla p + \mu\nabla^2\vec{u} - \rho\vec{g}\left[\beta_T(T - T_0)\right] \tag{2}$$

In the above equations, ρ, c_P, k, p, μ, β_T, T, $\vec{g}$ and $\vec{u}$ are respectively the density, specific heat, thermal conductivity, pressure, dynamic viscosity, thermal expansion coefficient, temperature, gravity vector and the flow velocity. The internal radiative heat transfer in the sapphire crystal is simulated by accounting the radiative heat source Q_R in Eq. (1). The P1 approximation model, which relies on the hypothesis that the participating medium is optically thick, is applied in the present case. The optical thickness varies between 2.4 and 40 as function on the dimension of the growing sapphire ingot. The melt has been considered opaque in the present computations.

The radiative heat source in Eq. (1) is given by:

$$Q_R = a\left(G - 4n^2\sigma T^4\right) \tag{3}$$

where a is the absorption coefficient, n is the refractive index and σ is the Stefan-Boltzmann constant. The incident radiation G is computed by solving the following equation:

$$-\nabla\left(D_{P1}\nabla G\right) = a\left(G - 4n^2\sigma T^4\right) \tag{4}$$

where D_{P1} is P1 diffusion coefficient defined as:

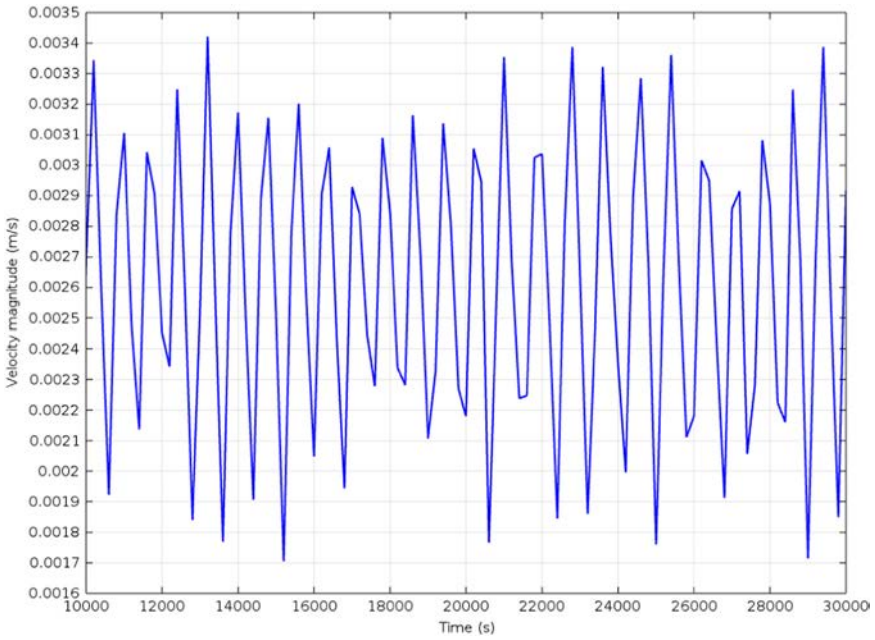

Fig. 4. Evolution in time of the velocity in the control point shown in Fig. 3b.

$$D_{P1} = \frac{1}{3a + b(3 - l_1)} \tag{5}$$

In the above equation, b is the scattering coefficient and l_1 is the linear Legendre coefficient of the scattering phase function (the scattering effect is not considered in the present simulation). The radiative heat flux at the solid boundaries of the crystal, which are considered opaque, is given by:

$$\phi_R = \frac{\varepsilon}{2(2 - \varepsilon)}\left(4n^2\sigma T^4 - G\right) \tag{6}$$

where ε is the surface emissivity. The crystal-melt interface has been considered a black wall ($\varepsilon = 1$).

The release of the latent heat at the crystal-melt interface is given by the following equation:

$$\left(k_S \nabla T|_S - k_L \nabla T|_L\right)\cdot\vec{n} = \rho_S \cdot \Delta H \cdot V \tag{7}$$

where S and L denotes the solid and the liquid phases, and ΔH, V and $\vec{n}$ are, respectively, the latent heat of fusion, growth velocity and the normal vector at the interface.

The melt convection is driven by buoyancy and Marangoni effects. The Marangoni flow occurs at the free surface of the melt, due to the dependence of the interface tension on the temperature. This effect has been modeled by introducing the following boundary condition at the free surface of the melt:

$$\mu\frac{\partial u_s}{\partial n} = \gamma\frac{\partial T}{\partial s} \tag{8}$$

where u_s is the tangential component of the flow velocity, $\vec{s}$ and $\vec{n}$ are the tangential and the normal unit vectors to the free surface, r is the radial coordinate and $\gamma = d\sigma_S/dT$ is the derivative of the surface tension as function of the temperature ($\gamma = -3.5\cdot10^{-5}$ N/m·K from Ref. [5]).

The transient modeling of the solidification process is performed by using the deformed mesh technique. There are three moving interfaces in the present model: the crystal-melt interface which takes the shape of the solidification isotherm, the crystal-gas interface which gives the external shape of the crystal, and the melt-gas interface which is moving down during the crystallization process. The mesh used for the local simulation has 10,000 triangular elements. The maximum time step in the transient simulations is 0.5 s. The physical properties of alumina in the solid and liquid phases are taken from [5]. Our measurements for the absorption coefficient of Ti-doped crystals show a mean value of a = 80 m^{-1} corresponding to C = 0.1% titanium concentration in the sample.

3. Results

Numerical modeling is performed in the case of crystals grown in crucibles of 15 cm and 30 cm in diameter. The computed shape of the crystal-melt interface is compared to the experimental visualization of the growth interface. In these experiments, the crystallization process was stopped by quickly pulling out the crystal from the melt. Fig. 2 shows the shape of the crystals obtained by interrupting the growth process at time t = 31 h (Fig. 2a) and, respectively, at time t = 67 h (Fig. 2b). The crystal-melt interface has a convex-concave shape with a large curvature. The non-dimensional interface deflection defined as the ratio between the deflection and crystal radius ($\tau = f/r_c$) increases during the crystallization process: τ = 4.5 cm/2.9 cm = 1.55 at time t = 31 h and τ = 11 cm/4.3 cm = 2.55 at time t = 67 h.

3.1. Convective effects

The effect of the convection on the interface shape is studied in Fig. 3. The computations are performed at the beginning of the growth process by neglecting the internal radiation in the crystal. The flow is driven by buoyancy and Marangoni effects. The values of the Grashof ($Gr = g\beta_T \Delta T R^3 \rho^2/\mu^2$) and Marangoni ($Ma = -\gamma\rho c_P \Delta T_S R_S/\mu k$) numbers at the beginning of the crystallization process are: Gr = $2\cdot10^4$ and Ma = 3200. ΔT and ΔT_S represent the temperature difference in the melt and, respectively, at the free surface of the liquid, R is the crucible radius and R_S is the radial dimension of the free surface of the melt. The buoyancy convection consists of two main vortices (Fig. 3a). In the primary vortex, the fluid downwards at the sample center and moves up near the crucible wall. The secondary vortex has an opposite direction and is located near the free

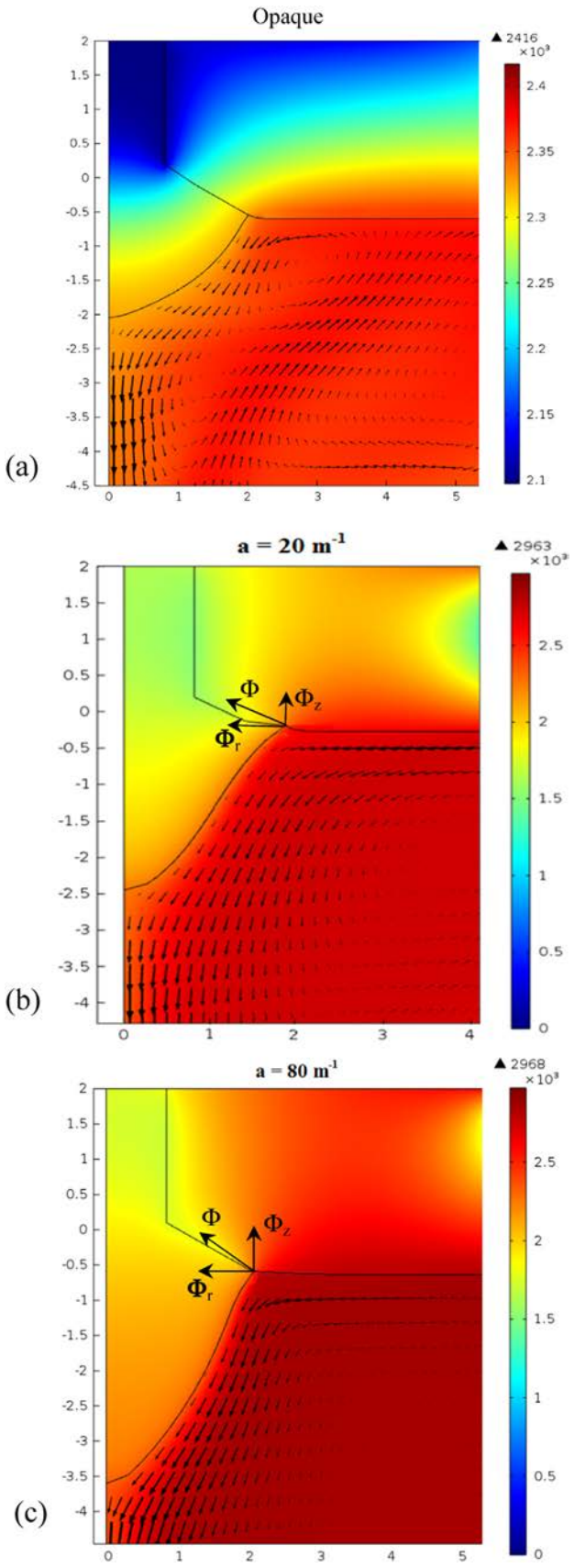

Fig. 5. Effect of the internal radiation on interface shape: (a) without internal radiation in the crystal (τ = 1.5 cm/2 cm = 0.75); (b) with internal radiation for non-doped sapphire crystal (a = 20 m^{-1}, τ = 2.3 cm/2 cm = 1.15); (c) with internal radiation for Ti-doped sapphire crystal (a = 80 m^{-1}, τ = 3 cm/2 cm = 1.5). Color map shows the temperature field (K). (For interpretation of the references to color in this figure legend, the reader is referred to the web version of this article.).

surface of the melt. The transient computation shows an unsteady convection with a flow pattern which is changing periodically in time (see the plot of the velocity in a control point illustrated in Fig. 4). This is explained by the high value of the Prandtl number (Pr = 14.5) featuring a strong interaction between the thermal and the flow field. Fig. 3b shows the results obtained by accounting the Marangoni effect. The thermo-capillary convection is located at the free surface of the melt and has opposite direction to the flow in the secondary vortex. The intensity of the Marangoni flow depends on the radial temperature gradient along the liquid-gas interface, which increases significantly during the first stage of the crystallization process, when the crystal grows faster in the radial direction. The intense flow near the triple crystal-melt-gas line changes the shape of the solidification interface, which becomes convex-concave (see Fig. 3b). The dimensionless interface deflection increases due to the Marangoni effect from τ = 0.57 (Fig. 3a) to τ = 0.73 (Fig. 3b).

3.2. Internal radiative effects

The effect of the internal radiation on the crystal-melt interface shape is shown in Fig. 5. The computations including the Marangoni effect are performed in three cases: a) without internal radiation in the crystal (opaque crystal), b) with internal radiation in the case of non-doped sapphire crystal (absorption coefficient a = 20 m^{-1}) and c) with internal radiation in the case of Ti-doped sapphire crystal (absorption coefficient a = 80 m^{-1}). The interface shape is slightly affected by the flow, since the Marangoni convection is less intense at the beginning of the growth process. Fig. 5a shows the results obtained for an opaque crystal. The thermal conductivity in the solid phase k_S = 6 W/m·K is higher than in the liquid phase k_L = 3 W/m·K. This leads to a convex (toward the melt) shaped interface with a relatively small curvature: τ = 1.5 cm/2 cm = 0.75. The cases computed by accounting the absorption coefficient show that the interface shape is significantly affected by the internal radiative transfer (see Fig. 5b and c). For a participating medium, the heat is conducted more easily from the melt to the crystal, since the radiative energy is absorbed and re-emitted by the growing ingot. Therefore, the heat flux through the crystal increases, leading to a significant increase of the effective thermal conductivity of the sapphire crystal. The ingot grows faster on the axial direction (z-axis) as compared to the opaque case. That explains the increased interface deflection obtained for the cases computed by accounting the internal radiative effect (Fig. 5b and c). Numerical results show that the non-dimensional interface deflection increases for a Ti-doped crystal as compared to a non-doped crystal: τ = 2.3 cm/2 cm = 1.15 (Fig. 5b) and τ = 3 cm/2 cm = 1.5 (Fig. 5c). That can be explained by accounting the heat flux balance in the vicinity of the triple crystal-melt-gas point. According to Rosseland's formula, the effective thermal conductivity of a participating medium decreases with increasing absorption coefficient:

$$k_{eff} = k_{opaque} + \frac{16n^2\sigma T^3}{3a} \tag{9}$$

The plot in Fig. 5b shows that at lower absorption coefficient (higher k_{eff}), the heat flux transferred from the melt to the crystal in the vicinity of the triple point is preferentially oriented to the crystal (radial direction). The ratio between the radial and the vertical component of the heat flux ϕ_r/ϕ_z is higher if compared to the case shown in Fig. 5c. The crystal grows faster on the radial direction at low absorption coefficient, so the dimensionless interface deflection is smaller in this case.

3.3. Comparison to experiments

The results obtained from modeling the first visualization

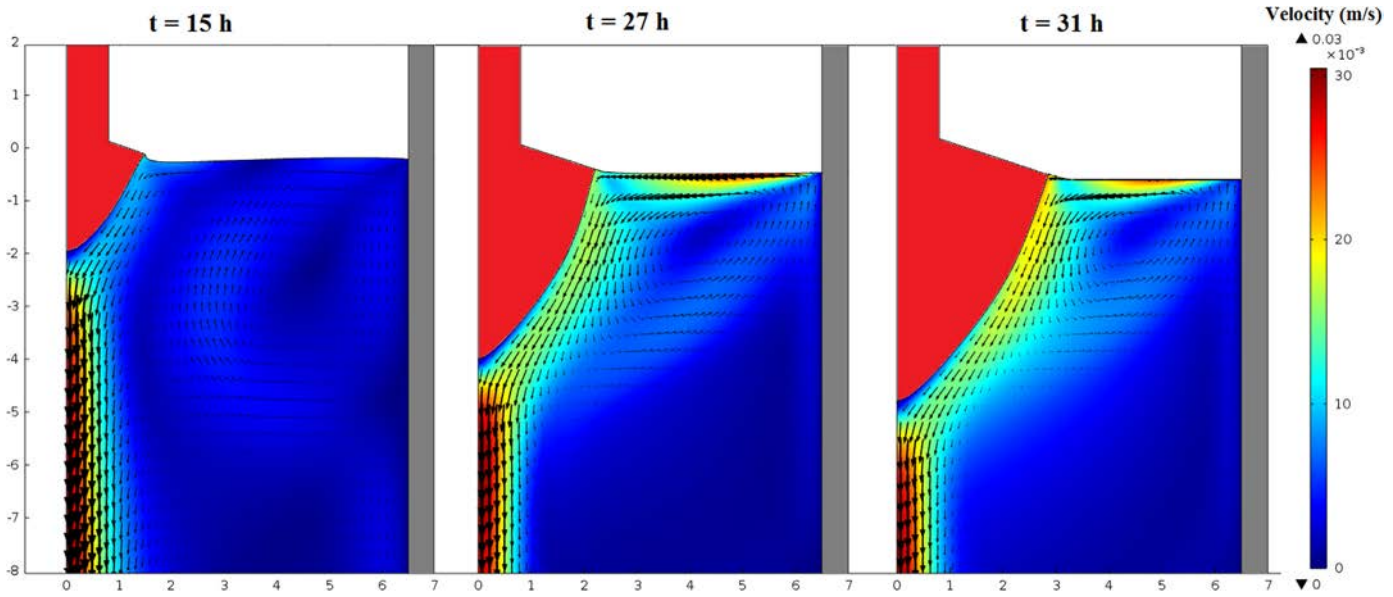

Fig. 6. Evolution in time of the velocity field and interface shape in the case of the first visualization experiment. Non-dimensional deflection of the growth interface: $\tau = 1.85$ cm/1.5 cm = 1.23 at t = 15 h, $\tau = 3.4$ cm/2.26 cm = 1.5 at t = 27 h and $\tau = 4.28$ cm/2.8 cm = 1.53 at t = 31 h.

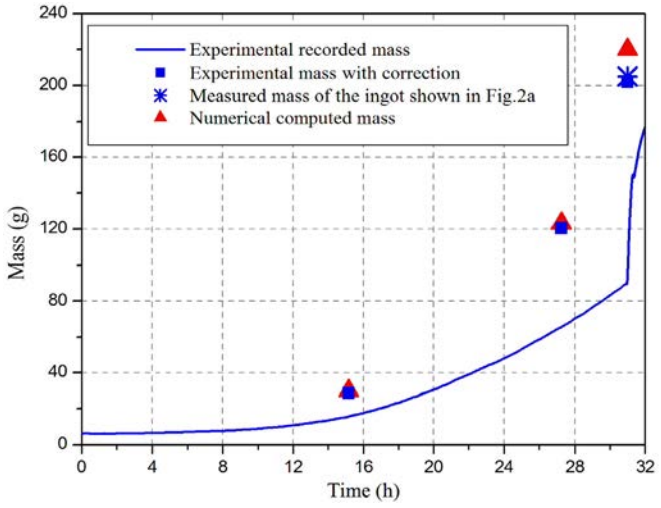

Fig. 7. Comparison of the recorded mass of the crystal (continuous line), the experimental mass with correction (squares) and the numerical computed mass (triangles).

Fig. 8. Formation of a plateau and temporal concave shape of the crystal observed during the first stage of growth in crucibles of d = 30 cm in diameter.

experiment (Fig. 2a) are shown in Fig. 6. The evolution in time of the velocity field shows that the intensity of the Marangoni convection increases during the first stage of the growth process (t = 0 – 30 h). The convection is characterized by two main flow cells: the axial flow with downward motion of the fluid at the centerline, and a clockwise vortex located near the free surface of the melt (see results at time t = 15 h). As the crystal radius increases, the radial temperature gradient at the melt-gas interface increases, resulting in a strengthening of the Marangoni flow (see the plot at time t = 27 h). The secondary vortex is completely overwhelmed by the Marangoni convection which reinforces the flow in the main vortex. The non-dimensional interface deflection increases from $\tau = 1.85$ cm/1.5 cm = 1.23 at time t = 15 h to $\tau = 4.28$ cm/2.8 cm = 1.53 at t = 31 h. These results are in agreement with the experimental measurement of the interface curvature showing a value $\tau = 4.5$ cm/2.9 cm = 1.55 at time t = 31 h (see Fig. 2a). The convex-concave shape of the interface is more obvious in the experiment as compared to our computations (see Fig. 2a and Fig. 6 at time t = 31 h).

Numerical simulation is also validated by comparing the computed mass of the growing crystal to experimental measurements. The mass of the crystal is the sum of the floated and submerged parts:

$$M = M_1 + M_2 \tag{10}$$

The measured mass of the submerged part of the crystal is smaller than the actual quantity due to the Archimedes force. The recorded mass of the crystal can be expressed as:

$$M_{exp} = M_1 + M_2' \tag{11}$$

where the apparent mass of the submerged crystal is given by:

$$M_2' = M_2 - \rho_L V_2 \tag{12}$$

The volume of the immersed crystal can be evaluated by assuming a conical shape of the crystal-melt interface:

$$V_2 = \frac{\pi r_c^2 f}{3} \tag{13}$$

Therefore, we get the following expression for M_{exp}:

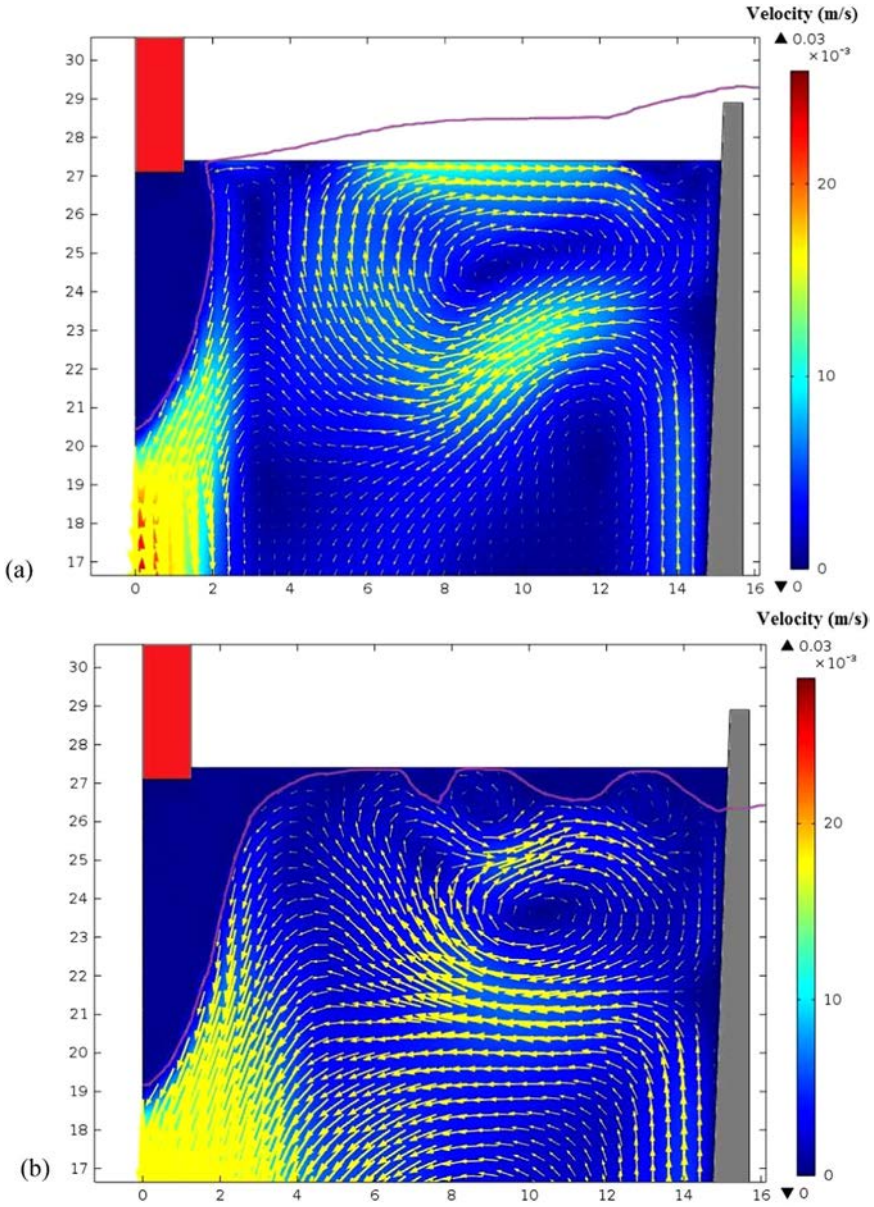

Fig. 9. Evolution in time of the velocity field and solidification isotherm (in red) at the beginning of the growth process: (a) after seeding; (b) after $\Delta t = 0.15$ h. Results carried out from global modeling of the Kyropoulos furnace. Crucible diameter d = 30 cm. (For interpretation of the references to color in this figure legend, the reader is referred to the web version of this article.).

$$M_{exp} = M_1 + M_2 - \frac{\pi r_c^2 f \rho_L}{3} = M - \frac{\pi r_c^2 f \rho_L}{3} \tag{14}$$

The correction of the experimental mass $\Delta M = \pi r_c^2 f \rho_L / 3$ can be evaluated by using the computed values for the interface deflection (f) and crystal radius (r_c). Fig. 7 shows the comparison of the recorded mass of the crystal (M_{exp}) and the computed mass. We obtain a good agreement between the numerical values and the experimental data with correction ($M_{exp} + \Delta M$). The computed mass is overestimated by ≈18 g at the end of the growth process (t = 31 h) if compared with the measured mass of the ingot $M_{ingot} = 205$ g.

3.4. Plateau formation

Some experiments conducted in crucibles of 30 cm in diameter have shown the formation of a plateau during the first stage of crystallization (see Fig. 8). The formation of so-called "temporal concave of the crystal" or "remelting zone" is often observed during the growth of large size Kyropoulos ingots. Several hypothesis have been formulated in order to explain this effect. Demina et al. [4] suggested that the formation of the remelting zone is related to the secondary flow cell, while Gao et al. [9] considered that it is an effect of the Marangoni flow.

Our global and local simulations of the growth process in crucibles of 30 cm in diameter, show that the plateau formation is related to unfavorable thermal conditions during the first stage of the crystallization. The global simulation is firstly applied to compute the thermal and the flow field in the furnace at the beginning of the crystallization process. The computations are performed in some particular conditions which promote the plateau formation. Fig. 9 shows the evolution in time of the velocity field and the solidification isotherm after the seeding stage. The velocity distribution in the alumina charge is computed at temperatures greater than the melting point. The external shape of the crystal and the evolution in time of the solidification front are not determined in the present case. Fig. 9a shows that the

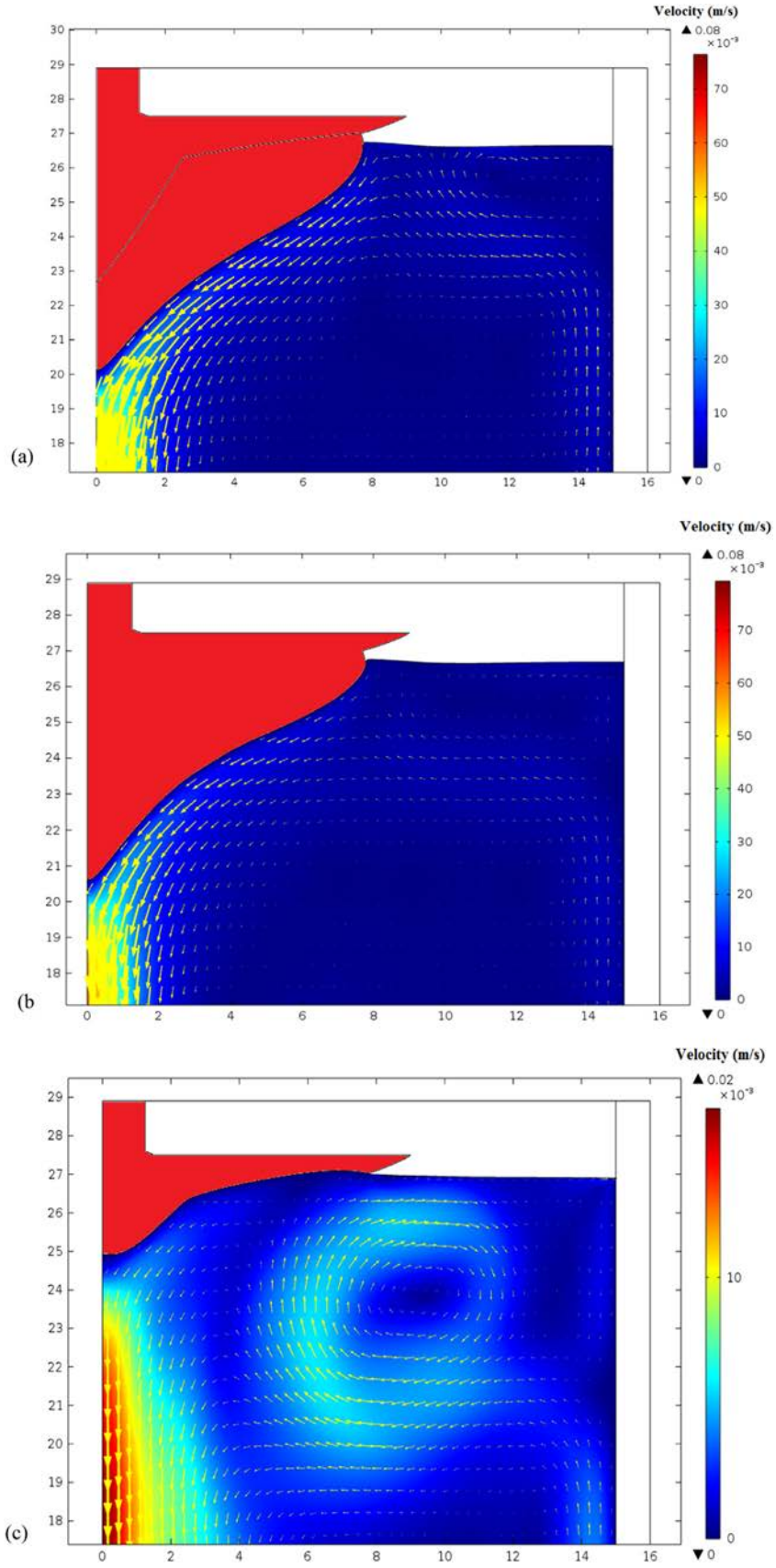

Fig. 10. Evolution in time of the external shape of the crystal and growth interface in the case: (a) with Marangoni convection; (b) without Marangoni convection; (c) without internal radiative effect in the crystal. Crucible diameter d = 30 cm.

solidification isotherm is nearly parallel to the free surface of the melt. Since the Marangoni flow is weak at the beginning of the growth process, the flow pattern consists of two cells with the secondary vortex developed near the melt-gas interface. Fig. 9b shows the results obtained after $\Delta t = 0.15$ h. As the power in the heater is decreased, the crystallization occurs very quickly in the radial direction, leading to plateau formation. Small solid zones appearing at the melt-gas interface are remelted by the convection. This generates a very unstable flow at the top surface of the melt, characterized by small opposite vortices (see Fig. 9b). It is concluded that a thermal field with isotherms nearly parallel to the free surface of the melt is likely to produce the plateau formation during the first stage of the growth process.

Local simulation is then applied to study the influence of the Marangoni flow on the crystal shape, after the plateau formation. The deformed mesh technique is used to compute the evolution in time of the crystal shape and the growth interface. The computations are started by considering an initial shape of the crystal, with plateau (blue line in Fig. 10a), which corresponds to the final result shown in Fig. 9b. The cases computed with and without Marangoni flow (Fig. 10a and b) show that the concave shape of the crystal is not influenced by the Marangoni convection (Ma = 5400). The flow intensity increases near the triple point due to the Marangoni effect, but the convection is not strong enough to influence the external shape of the crystal. The result plotted in Fig. 10c is carried out from a computation which neglects the internal radiative effect in the crystal. The curvature of the crystal-melt interface decreases significantly as compared to the simulated cases which account for the internal radiative effect: $\tau = 6.6$ cm/7.9 cm = 0.84 (Fig. 10a) and $\tau = 2$ cm/7.7 cm = 0.26 (Fig. 10c). The transient computation shows a remelting of the plateau in this case.

The present results show that the formation of a plateau and the temporal concave shape of the crystal are mainly related to unfavorable heat transfer conditions in the furnace. The flow can influence the shape of the growth interface, but cannot change significantly the external shape of the crystal.

4. Conclusions

Transient global and local modeling was performed in order to investigate the influence of the convective and internal radiative effects on the shape of the crystal-melt interface during the Kyropoulos growth of Ti-doped sapphire crystals. The modeling of the melt convection shows that the Marangoni flow reinforces the buoyancy flow at the sample axis, leading to an increased interface curvature. The intensity of the Marangoni convection increases during the first stage of the growth, affecting the shape of the growth interface which becomes convex-concave.

The internal radiative heat transfer in the sapphire crystal has a significant effect on the interface shape. The effective thermal conductivity of the crystal increases during the growth process, affecting the solidification interface which becomes conical. Numerical modeling shows that the non-dimensional interface deflection increases two times in the case of Ti-doped crystals (absorption coefficient $a = 80\ m^{-1}$) as compared to opaque crystals. Numerical modeling of the crystallization process in crucibles of 15 cm in diameter is compared to experimental visualization of the growth interface. A good agreement is obtained for the computations of interface deflection and crystal mass.

The formation of a plateau, which was observed in some experiments carried out in crucibles of 30 cm in diameter, has been investigated by global and local modeling. The global computations of the temperature and flow field at the beginning of crystallization process, show that this undesirable effect is due to unfavorable heat transfer conditions in the furnace. The crystal grows very fast on the radial direction when the solidification isotherm is nearly parallel to the free surface of the melt. After the plateau formation, the crystal exhibits a concave shape, then the ingot diameter increases again until the nominal value is reached. Computations performed with and without Marangoni convection show no significant effect of the flow on the external shape of the crystal. On contrary, the internal radiative heat exchanges can influence the temporal concave shape of the crystal.

Acknowledgments

This research is supported by the FUI Titan-Saphir grant sponsored by the French Government. The authors are grateful to K. Lebbou, C. Pezzani and G. Alombert-Goget for their help.

References

[1] F. Moulton, J. Opt. Soc. Am. B3 (1986) 125.
[2] A. Nehari, A. Brenier, G. Panzer, K. Lebbou, J. Godfroy, S. Labor, H. Legal, G. Cheriaux, J.P. Chambaret, T. Duffar, R. Moncorge, Cryst. Growth Des. 11 (2) (2011) 445.
[3] S.E. Demina, E.N. Bystrova, V.S. Postolov, E.V. Eskov, M.V. Nikolenko, D. A. Marshanin, V.S. Yuferev, V.V. Kalaev, J. Cryst. Growth 310 (2008) 1443.
[4] S.E. Demina, V.V. Kalaev, J. Cryst. Growth 320 (2011) 23.
[5] C.H. Chen, J.C. Chen, C.W. Lu, C.M. Liu, J. Cryst. Growth 318 (2011) 162.
[6] C.H. Chen, J.C. Chen, C.W. Lu, C.M. Liu, J. Cryst. Growth 352 (2012) 9.
[7] W.J. Lee, Y.C. Lee, H.H. Jo, Y.H. Park, J. Cryst. Growth 324 (2011) 248.
[8] C. Chen, H.J. Chen, W.B. Yan, C.H. Min, H.Q. Yu, Y.M. Wang, P. Cheng, C.C. Liu, J. Cryst. Growth 388 (2014) 29.
[9] Y. Gao, X. Gao, J. Lu, J. Sci. 2 (8) (2015) 146.